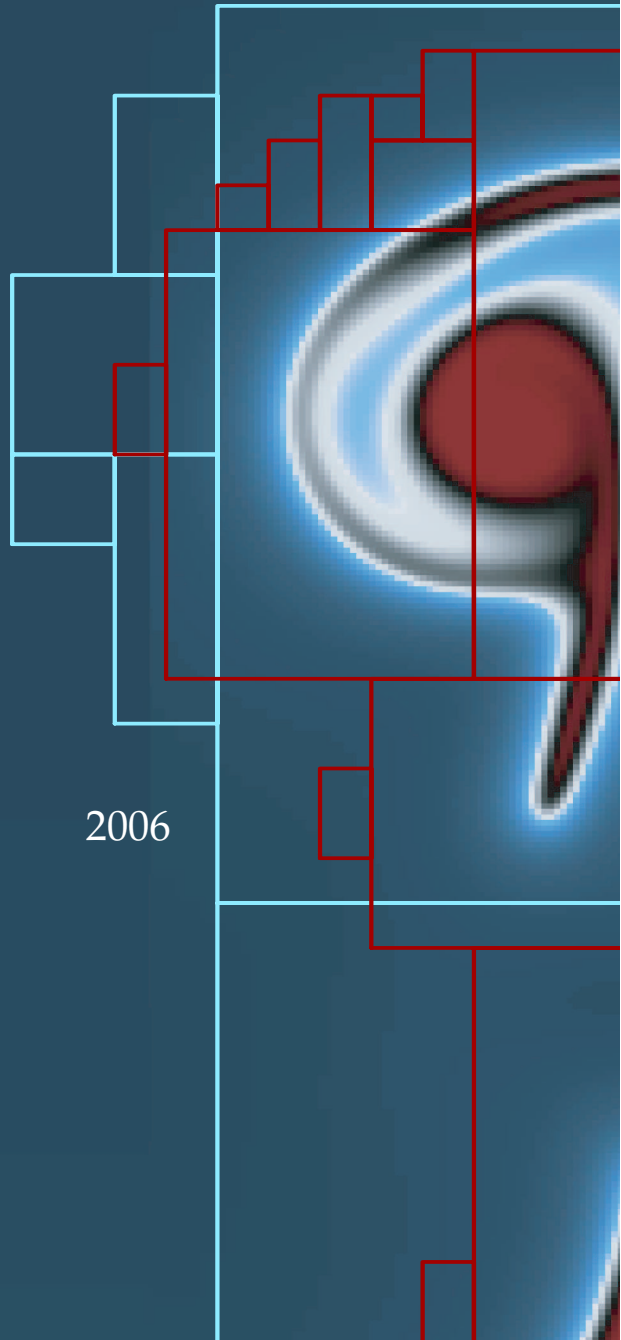


*Communications in
Applied
Mathematics and
Computational
Science*

Volume 1

No. 1

2006



**THE FAST SINC TRANSFORM
AND IMAGE RECONSTRUCTION FROM
NONUNIFORM SAMPLES IN k -SPACE**

LESLIE GREENGARD, JUNE-YUB LEE AND SOUHEIL INATI



mathematical sciences publishers

THE FAST SINC TRANSFORM AND IMAGE RECONSTRUCTION FROM NONUNIFORM SAMPLES IN k -SPACE

LESLIE GREENGARD, JUNE-YUB LEE AND SOUHEIL INATI

A number of problems in image reconstruction and image processing can be addressed, in principle, using the sinc kernel. Since the sinc kernel decays slowly, however, it is generally avoided in favor of some more local but less precise choice. In this paper, we describe the fast sinc transform, an algorithm which computes the convolution of arbitrarily spaced data with the sinc kernel in $O(N \log N)$ operations, where N denotes the number of data points. We briefly discuss its application to the construction of optimal density compensation weights for Fourier reconstruction and to the iterative approximation of the pseudoinverse of the signal equation in MRI.

1. Introduction

A number of imaging modalities require the inversion of the equation

$$s(n) = \int_V \rho(\mathbf{r}) e^{2\pi i \mathbf{k}(n) \cdot \mathbf{r}} d\mathbf{r}, \quad (1)$$

where $\mathbf{k}(n)$ denotes the location of the n th measurement in the frequency domain (“ k -space”) and \mathbf{r} denotes position in the image domain. It will be convenient below to write this in operator form as

$$\mathbf{s} = \mathcal{H}\rho(\mathbf{r}), \quad (2)$$

where \mathcal{H} is the “continuous-to-discrete” Fourier operator which maps the image space to the signal space. (In standard magnetic resonance imaging, $\rho(\mathbf{r})$ is the proton spin density.)

We are particularly concerned with nonuniform sampling schemes, where the points $\{\mathbf{k}(n)\}$ do not lie on a regular grid. The inversion of (2) is, of course, an

Keywords: sinc interpolation, fast transform, nonuniform fast Fourier transform, density compensation weights, iterative methods, Fourier analysis, image reconstruction, magnetic resonance imaging (MRI).

Greengard was supported in part by the U.S. Department of Energy under contract DE-FG02-00-ER25053. Inati was supported in part by the McKnight Foundation, the Seaver Foundation, and the Swartz Foundation.

inherently ill-posed problem; the space of all possible densities $\rho(\mathbf{r})$ is infinite dimensional, while the vector of measurements $\{s(n)\}$ is finite dimensional. In the present paper, we concentrate on two possible approaches to reconstruction, leaving a more general discussion to [12].

Scheme 1. The first reconstruction scheme relies on the inverse Fourier transform

$$\rho(\mathbf{r}) = \iint s(\mathbf{k})e^{-2\pi i\mathbf{k}\cdot\mathbf{r}}d\mathbf{k}, \quad (3)$$

or, more precisely, its approximation at M locations \mathbf{r}_m via

$$\rho(\mathbf{r}_m) \approx \sum_{n=1}^N s(n)e^{-2\pi i\mathbf{k}(n)\cdot\mathbf{r}_m}w_n. \quad (4)$$

The computation of the sum (4) for every location appears to require $O(NM)$ operations. Using the nonuniform fast Fourier transform (NUFFT), however, this can be accomplished using $O((N+M)\log(N+M))$ operations. This is now a relatively mature technology [2; 6; 8; 9; 11; 14; 15; 17].

In (4), the values $\{w_n\}$ can be considered quadrature weights, and it is shown in [3; 12] that an optimal set of weights is given by the formula

$$\frac{1}{w_n} = \sum_{m=1}^N \text{sinc}^2(\mathbf{k}(m) - \mathbf{k}(n)). \quad (5)$$

Here, $\text{sinc}(k) \equiv \sin(\pi k)/\pi k$ and, in d dimensions, we define $\text{sinc}(\mathbf{k}) = \text{sinc}(k_1) \cdot \text{sinc}(k_2) \cdots \text{sinc}(k_d)$, where $\mathbf{k} = (k_1, k_2, \dots, k_d)$. While the evaluation of these weights appears to require $O(N^2)$ operations, the fast sinc^2 transform, described below, makes use of the NUFFT to reduce the cost to $O(N \log N)$.

Scheme 2. A second class of reconstruction schemes is based directly on the signal equation (2). The minimum-norm least-squares solution to this problem, denoted by $\hat{\rho}(\mathbf{r})$, can be found by applying \mathcal{H}^+ , the pseudo-inverse [10] of the operator \mathcal{H} , to the signal. Following the discussion of [19], we write

$$\hat{\rho}(\mathbf{r}) = \mathcal{H}^+\mathbf{s} = \mathcal{H}^\dagger(\mathcal{H}\mathcal{H}^\dagger)^+\mathbf{s}, \quad (6)$$

where \mathcal{H}^\dagger is the adjoint of \mathcal{H}

$$[\mathcal{H}^\dagger\mathbf{a}](\mathbf{r}) = \sum_n e^{-2\pi i\mathbf{k}(n)\cdot\mathbf{r}}a(n),$$

where $\mathbf{a} = (a(1), \dots, a(n))$ and $(\mathcal{H}\mathcal{H}^\dagger)^+$ is the pseudoinverse of $\mathcal{H}\mathcal{H}^\dagger$.

Given the N sample points $\{\mathbf{k}(n)\}$ in k -space, it is straightforward to verify that

$$(\mathcal{H}\mathcal{H}^\dagger)_{mn} = \text{sinc}(\mathbf{k}_m - \mathbf{k}_n). \quad (7)$$

For notational convenience, we let $M = \mathcal{H}\mathcal{H}^\dagger$. The desired function $\hat{\rho}(\mathbf{r})$ in (6) can then be computed in two steps:

(1) Solve the system

$$M\mathbf{a} = \mathbf{s} \tag{8}$$

(2) Compute

$$\hat{\rho}(\mathbf{r}) = \mathcal{H}^\dagger \mathbf{a}.$$

The matrix M , however, may be ill-conditioned, with the precise condition number depending on the distribution of the sample points. (If two sample points coincide, for example, M is actually singular.) Thus, it is natural, as in [19], to use the pseudoinverse construction

$$\mathbf{a} = M^+ \mathbf{s},$$

which can be computed using the singular value decomposition (SVD) at a cost of $O(N^3)$ work. For this, some additional assumptions need to be made as to the choice of regularization [10]. Alternatively, one can attempt an iterative solution of (8). In [5], the authors suggest applying the conjugate gradient method, which is suitable for symmetric positive definite matrices. Since the cost of applying M to a vector is $O(N^2)$ work, the total cost of solving the system is of the order $O(J \cdot N^2)$, where J denotes the number of iterations.

Remark 1. Note that (4) can be written as

$$\rho(\mathbf{r}) \approx \mathcal{H}^\dagger W \mathbf{s}$$

where W is the diagonal matrix of quadrature weights. Thus, the quadrature approach based on the inverse Fourier transform can be viewed as a diagonal approximation ($W\mathbf{s}$) of the pseudoinverse construction ($M^+\mathbf{s}$). As a result, W serves as a good preconditioner for the conjugate gradient method applied to (8).

In summary, both Scheme 1 and Scheme 2 would benefit from appropriate fast algorithms: the optimal weights require a single convolution with the kernel $\text{sinc}^2(\mathbf{k})$ and the iterative solution of the signal equation requires repeated convolution with the kernel $\text{sinc}(\mathbf{k})$.

2. The fast sinc transform

Suppose now that we are given two sets of points $\{\mathbf{k}_n = (k_n^1, k_n^2, \dots, k_n^d) \mid n = 1, \dots, N\}$, and $\{\mathbf{v}_m = (v_m^1, v_m^2, \dots, v_m^d) \mid m = 1, \dots, M\}$, which we think of as located in the frequency domain in d dimensions. The point sets $\{\mathbf{k}_n\}$ and $\{\mathbf{v}_m\}$ may or may not coincide. We define the d -dimensional sinc and sinc^2 transforms

by

$$U_m = \sum_{n=1}^N q_n \operatorname{sinc}(\mathbf{k}_n - \mathbf{v}_m) \quad \text{and} \quad W_m = \sum_{n=1}^N q_n \operatorname{sinc}^2(\mathbf{k}_n - \mathbf{v}_m), \quad (9)$$

respectively. Clearly, the naive computation of either U_m or W_m from q_n requires $O(M \cdot N)$ work. Since the transforms take the form of convolutions, it is perhaps not surprising that the Fourier transform will play a role in the fast algorithm. Since the data are not assumed to lie on a regular mesh, however, an essential ingredient will be the nonuniform fast Fourier transform (NUFFT), mentioned above. In its most general form, the NUFFT of “type 3” computes sums of the form

$$G_j = \sum_{p=1}^P g_p e^{-i\mathbf{k}_j \cdot \mathbf{x}_p}, \quad (10)$$

for $j = 1, \dots, J$ or

$$g_p = \sum_{j=1}^J G_j e^{+i\mathbf{k}_j \cdot \mathbf{x}_p}, \quad (11)$$

for $p = 1, \dots, P$ in $O((J + P) \log(J + P))$ operations to any desired precision. We will refer to equation (10) as the forward NUFFT. We can think of it as a discretization of the continuous Fourier transform,

$$G(\mathbf{k}) = \int_{-\infty}^{\infty} \cdots \int_{-\infty}^{\infty} g(\mathbf{x}) e^{-2\pi i \mathbf{x} \cdot \mathbf{k}} d\mathbf{x} = \mathcal{F}g(\mathbf{x}), \quad (12)$$

using nonuniformly sampled discretization points and evaluated at nonuniformly sampled frequencies. We will refer to (11) as the adjoint NUFFT. We can think of it as a discretization of the continuous inverse Fourier transform,

$$g(\mathbf{x}) = \int_{-\infty}^{\infty} \cdots \int_{-\infty}^{\infty} G(\mathbf{k}) e^{2\pi i \mathbf{x} \cdot \mathbf{k}} d\mathbf{k} = \mathcal{F}^{-1}G(\mathbf{k}), \quad (13)$$

using nonuniformly sampled frequencies and evaluated at nonuniformly sampled discretization points.

Remark 2. The nomenclature *inverse* NUFFT would be misleading since, in the discrete case with nonuniform points, it is not the inverse of the forward transform.

Remark 3. The NUFFT has been used previously in order to accelerate iterative methods for the signal equation (1). In [5; 20], for example, the signal equation (or an analog) was discretized and the resulting linear system was solved using the conjugate gradient method applied to the normal equations. Their approach, however, did not make use of the sinc kernel.

The development of the fast sinc or sinc² transform now follows. For the sake of concreteness, we restrict our attention to the two-dimensional case, but the approach is clearly independent of dimension. First, we observe that the first equation in (9) can be viewed as the evaluation of the function

$$U(\mathbf{v}) = \int_{-\infty}^{\infty} \int_{-\infty}^{\infty} \text{sinc}(\mathbf{v} - \mathbf{k}) H(\mathbf{k}) d\mathbf{k} \tag{14}$$

at the points \mathbf{v}_m , due to the singular “source” distribution

$$H(\mathbf{k}) = \sum_{n=1}^N q_n \delta(\mathbf{k} - \mathbf{k}_n).$$

This follows from the elementary properties of the δ -function. From the convolution theorem we have that $U(\mathbf{v})$ is given by

$$U(\mathbf{v}) = \int_{-\infty}^{\infty} \int_{-\infty}^{\infty} u(\mathbf{x}) e^{-2\pi i \mathbf{x} \cdot \mathbf{v}} d\mathbf{x} \tag{15}$$

with

$$u(\mathbf{x}) = \mathcal{F}^{-1} \text{sinc}(\mathbf{k}) \cdot \mathcal{F}^{-1} H(\mathbf{k}). \tag{16}$$

The latter two functions can be easily computed. The inverse Fourier transform $\mathcal{F}^{-1} \text{sinc}(\mathbf{k})$ in two dimensions is simply

$$\Pi(\mathbf{x}) = \begin{cases} 0 & \text{if } |x_1| > 1/2 \text{ or } |x_2| > 1/2, \\ 1 & \text{if } |x_1| < 1/2 \text{ and } |x_2| < 1/2, \end{cases} \tag{17}$$

where $\mathbf{x} = (x_1, x_2)$. Further, it is easy to see that

$$h(\mathbf{x}) = \mathcal{F}^{-1} H(\mathbf{k}) = \sum_{n=1}^N q_n e^{2\pi i \mathbf{x} \cdot \mathbf{k}_n}. \tag{18}$$

Thus, we can compute $U(\mathbf{v}_m)$ from (15)-(18):

$$U(\mathbf{v}_m) = \int_{-1/2}^{1/2} \int_{-1/2}^{1/2} h(\mathbf{x}) e^{-2\pi i \mathbf{x} \cdot \mathbf{v}_m} d\mathbf{x}. \tag{19}$$

This result is certainly classical.

2.1. Quadrature considerations. Equation (19) is an exact relation, and it remains only to discretize the integral. Doing so is straightforward, because $h(\mathbf{x})$ consists of a collection of exponential functions with maximum frequency given by $K_{\max} = \max_n \|\mathbf{k}_n\|_{L^1}$. Furthermore, we are only interested in computing $U(\mathbf{v}_m)$ itself up to the frequency K_{\max} so that the term $e^{-2\pi i \mathbf{x} \cdot \mathbf{v}_m}$ also has a maximal frequency content given by K_{\max} . Thus, the integrand in (19) is a band-limited function with

band limit $2 \cdot K_{\max}$. Nyquist sampling (two points per oscillation) requires that an accurate quadrature in two dimensions use at least $(4K_{\max})^2$ points.

Gauss–Legendre quadrature [4] is particularly useful in this context. While this approach is more involved than the trapezoidal rule or the rectangle rule, it achieves much higher order accuracy. More precisely, the P -point Gauss–Legendre rule can be defined by P weights $\{q_p\}$ and nodes $\{x_p\}$ so that the relation

$$\int_{-1}^1 x^n dx = \sum_{p=1}^P q_p x_p^n$$

is exactly satisfied for $n = 0, \dots, 2P - 1$. This yields a $2P \times 2P$ nonlinear system. Fortunately, the weights and nodes are easy to compute using standard software such as the Fortran routine `gaussq.f` from NETLIB (<http://www.netlib.org>). The weights are positive, but the nodes are not equally spaced, tending to cluster at the endpoints of the interval $[-1, 1]$. Given these weights and nodes, one of the remarkable features of Gauss–Legendre quadrature,

$$\int_{-1}^1 f(x) dx \approx \sum_{p=1}^P q_p f(x_p),$$

is that it satisfies the error estimate:

$$E = \left| \int_{-1}^1 f(x) dx - \sum_{p=1}^P q_p f(x_p) \right| < \frac{2^{2P+1} (P!)^4}{(2P+1)[(2P)!]^3} \cdot \max |f^{2P}(x)|,$$

where $f^{2P}(x)$ denotes the $2P$ -th derivative of the integrand. If the function $f(x)$ is band-limited by $2K_{\max}$, then $|f^{2P}(x)| < (4\pi K_{\max})^{2P}$. A modest amount of algebra then shows that the error E in using the P -point rule satisfies:

$$E < \frac{2\sqrt{\pi}\sqrt{P}}{(2P+1)} \left(\frac{1}{2e}\right)^{4P} \left(\frac{4\pi K_{\max}}{P}\right)^{2P} < \left(\frac{1}{e}\right)^{4P} \left(\frac{\pi K_{\max}}{P}\right)^{2P}.$$

Thus we see that, once P exceeds πK_{\max} , the error decays exponentially.

Using a tensor-product rule for the double integral, we have

$$\begin{aligned} U(\mathbf{v}_m) &= \int_{-1/2}^{1/2} \int_{-1/2}^{1/2} h(\mathbf{x}) e^{-2\pi i \mathbf{x} \cdot \mathbf{v}_m} d\mathbf{x} \\ &\approx \sum_{p_1=1}^P \sum_{p_2=1}^P h(x_{p_1}, x_{p_2}) e^{-2\pi i (x_{p_1}, x_{p_2}) \cdot \mathbf{v}_m} q_{p_1} q_{p_2} \end{aligned} \quad (20)$$

The error, as in the one-dimensional case, decays at an exponential rate once P exceeds πK_{\max} .

Remark 4. The usual weights and nodes are defined on the interval $[-1, 1]$ and we have scaled them to the interval $[-1/2, 1/2]$.

In summary, the fast sinc transform requires the adjoint NUFFT to compute $h(\mathbf{x})$ via (18) at the tensor product quadrature points. Given the values $h(x_{p_1}, x_{p_2})$, the forward NUFFT is used to compute (20). The amount of work is of the order $O((N + M + P^2) \log(N + M + P^2)) = O((N + M + K_{\max}^2) \log(N + M + K_{\max}^2))$. Since the quadrature used is spectrally accurate, the error in the fast sinc transform is dominated by the tolerance requested of the NUFFT. In most implementations, this is a user-controlled parameter and affects only the constant prefactor implicit in the $O((N + M) \log(N + M))$ notation.

Remark 5. For low accuracy, one could use the trapezoidal rule (a uniform mesh on $[-1/2, 1/2]$). The NUFFTs in this case are slightly more efficient, with a net savings of a factor of two or so in CPU time. The error is of the order $O(1/P^2)$, however, rather than exponentially small.

2.2. The fast sinc² transform. The theory underlying the sinc² transform is almost identical. The only change is that the inverse Fourier transform of $\text{sinc}^2(\mathbf{k})$ in two dimensions is $t(x_1) \cdot t(x_2)$ where

$$t(x) = \begin{cases} 0 & \text{if } |x| > 1, \\ 1 - |x| & \text{if } |x| < 1. \end{cases}$$

We therefore need to compute

$$W(\mathbf{k}) = \int_{-1}^1 \int_{-1}^1 h(x_1, x_2) t(x_1) t(x_2) e^{-2\pi i(x_1, x_2) \cdot \mathbf{k}} dx_1 dx_2. \quad (21)$$

Since the integrand is piecewise smooth, we maintain high accuracy by using four tensor product Gaussian quadrature rules (each with $P^2 > (\pi K_{\max})^2$ points) on the four quadrants $[-1, 0] \times [-1, 0]$, $[-1, 0] \times [0, 1]$, $[0, 1] \times [-1, 0]$, $[0, 1] \times [0, 1]$.

In summary, the fast sinc² transform requires the adjoint NUFFT to compute $h(\mathbf{x})$ via (18) at the tensor product quadrature points, followed by the forward NUFFT to compute (21) using tensor product Gaussian quadrature. The amount of work is again of the order $O((N + M + K_{\max}^2) \log(N + M + K_{\max}^2))$. Related algorithms that rely on the NUFFT for other convolution kernels are described in [16].

3. Results

We illustrate the performance of the algorithm in the context of magnetic resonance image reconstruction (MRI). In MRI, one seeks to produce a spatial map of the effective spin density $\rho(\mathbf{r})$ from raw complex-valued data $s(n) = s(\mathbf{k}(n))$ acquired in the Fourier domain. When the points $\mathbf{k}(n)$ are located on a Cartesian grid, the

N	T_{FST}	$T_{\text{FS}^2\text{T}}$	T_{dir}	Error
4096	0.05	0.26	9.1	$< 10^{-3}$
16384	0.11	0.36	145	$< 10^{-3}$
4096	0.09	0.34	9.1	$< 10^{-5}$
16384	0.19	0.61	145	$< 10^{-5}$

Table 1. Timing results for FST and FS^2T on an Archimedean spiral with $K_{\max} = 64$. N denotes the number of sampling points along the spiral, T_{FST} denotes the time required for the fast sinc transform, $T_{\text{FS}^2\text{T}}$ denotes the time required for the fast sinc² transform, and T_{dir} is the time required for the direct calculation. The direct calculation for sinc and sinc² are essentially the same, so only one timing is listed. Error is the requested tolerance for the NUFFT and is an upper bound on the L_2 error in the transform data. Calculations were carried out on a laptop computer with a 1.2GHz Pentium processor.

FFT is typically used to reconstruct the image according to (4) with constant weights $\{w_n\}$. Many modern techniques in MRI, however, including functional MRI, MR angiography, and abdominal imaging, use nonuniform samplings in \mathbf{k} -space which allow for significantly faster data acquisition rates [1; 18].

One prototypical acquisition scheme is the Archimedean spiral, which we truncate at $K_{\max} = 64$ and sample at N points according to the formula

$$\mathbf{k}_n = K_{\max} \sqrt{\frac{n}{N}} \left(\cos \left(3\pi K_{\max} \sqrt{\frac{n}{N}} \right), \sin \left(3\pi K_{\max} \sqrt{\frac{n}{N}} \right) \right).$$

Before discussing the image reconstruction process itself, we first use this sampling pattern in order to test the efficiency of our fast transforms. For this, the points \mathbf{k}_n serve as both the “source” locations and as the targets (the \mathbf{v}_m in the earlier discussion). Sample timings are given in Table 1.

While the fast transform timings scale as expected with problem size, they rely on the NUFFT algorithm from [14], which has not yet been fine-tuned for performance. We believe that an order of magnitude improvement can be obtained through careful code optimization.

To illustrate the performance of the algorithm in terms of image quality, we generate synthetic data $s(n)$ according to (1) from a standard test image (the Shepp–Logan phantom [7; 13]), depicted in Figure 1. We then consider two data acquisition patterns: an integer Cartesian grid truncated at $K_{\max} = 64$ and the Archimedean spiral above. Both data sets contained $128^2 = 16,384$ (complex) values. The

resulting reconstructions are shown in Figure 1. The top figure is based on the FFT using the Cartesian data, the lower left figure is based on the optimal weight reconstruction (Scheme 1) using (4), (5), and the lower right figure is obtained by using 5 iterations of the preconditioned conjugate gradient method (Scheme 2), with a diagonal preconditioner defined by the quadrature weights (5), as discussed in Remark 1. The total time for image reconstruction was approximately 0.2 seconds using the quadrature method (the lower left figure) and 1 second using the approximate pseudoinverse (lower right), the latter requiring 5 sinc transforms,

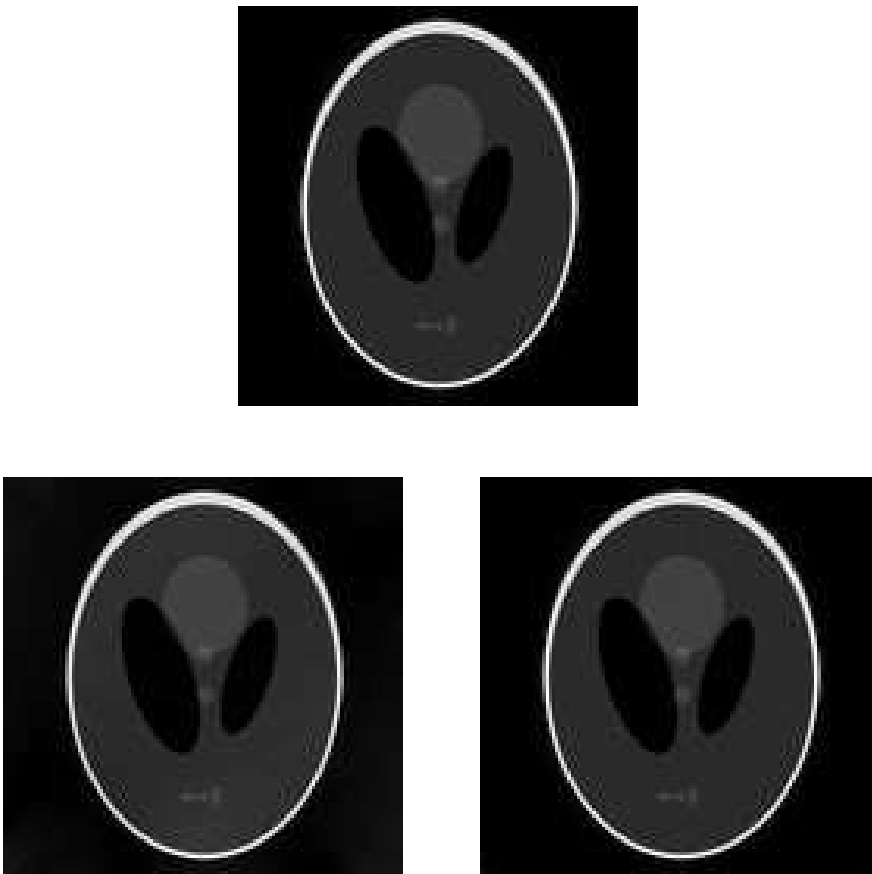


Figure 1. Image reconstruction from Cartesian (top) and spiral (bottom) k -space sampling. Note that the quadrature approximation (left) gives a very reasonable image. The pseudoinverse approximation (right) is nearly identical to that obtained in the Cartesian case.

one sinc^2 transform and one final NUFFT to apply the adjoint \mathcal{H}^\dagger . The FFT reconstruction is, of course, much faster — it required less than 0.01 seconds.

4. Discussion

We have constructed a fast algorithm for the (discrete) sinc and sinc^2 transforms which have immediate application in MR image reconstruction. The two algorithms will also accelerate, for example, the band-limited interpolation method of [3]. Since sinc convolution arises naturally in many signal and image processing contexts, we expect that the algorithms described here will be of fairly broad utility.

References

- [1] C. B. Ahn, J. H. Kim, and Z. H. Cho, *High speed spiral-scan echo planar imaging*, IEEE Trans. Med. Imag. **M1-5** (1986).
- [2] G. Beylkin, *On the fast Fourier transform of functions with singularities*, Appl. Comput. Harmon. Anal. **2** (1995), no. 4, 363–381. MR 96i:65122 Zbl 0838.65142
- [3] H. Choi and D. C. Munson, *Analysis and design of minimax-optimal interpolators*, IEEE Trans. Signal Processing **46** (1998), 1571–1579.
- [4] P. J. Davis and P. Rabinowitz, *Methods of numerical integration*, Computer Science and Applied Mathematics, Academic Press Inc., Orlando, FL, 1984. MR 86d:65004
- [5] B. Desplanques, D. J. Cornelis, E. Achten, R. Van de Walle, and I. Lemahieu, *Iterative reconstruction of magnetic resonance images from arbitrary samples in k -space*, IEEE Trans. Nuc. Sci. **49** (2002), 2268–2273.
- [6] A. Dutt and V. Rokhlin, *Fast Fourier transforms for nonequispaced data*, SIAM J. Sci. Comput. **14** (1993), no. 6, 1368–1393. MR 95d:65114 Zbl 0791.65108
- [7] C. L. Epstein, *Mathematics of medical imaging*, Prentice-Hall, Englewood Cliffs, NJ, 2003.
- [8] J. A. Fessler and B. P. Sutton, *Nonuniform fast Fourier transforms using min-max interpolation*, IEEE Trans. Signal Process. **51** (2003), no. 2, 560–574. MR 2003m:94024
- [9] K. Fourmont, *Non-equispaced fast Fourier transforms with applications to tomography*, J. Fourier Anal. Appl. **9** (2003), no. 5, 431–450. MR 2005b:65154 Zbl 1073.65151
- [10] G. H. Golub and C. F. Van Loan, *Matrix computations*, Johns Hopkins Series in the Mathematical Sciences, vol. 3, Johns Hopkins University Press, Baltimore, MD, 1989. MR 90d:65055
- [11] L. Greengard and J.-Y. Lee, *Accelerating the nonuniform fast Fourier transform*, SIAM Rev. **46** (2004), no. 3, 443–454. MR MR2115056 Zbl 1064.65156
- [12] S. Inati, J.-Y. Lee, L. Fleysher, R. Fleysher, and L. Greengard, *Iterative reconstruction of magnetic resonance images from non-uniform samples in k -space*, In preparation.
- [13] A. C. Kak and M. Slaney, *Principles of computerized tomographic imaging*, IEEE Press, New York, 1988. MR 90h:92005 Zbl 0721.92011
- [14] J.-Y. Lee and L. Greengard, *The type 3 nonuniform FFT and its applications*, J. Comput. Phys. **206** (2005), no. 1, 1–5. MR MR2135833 Zbl 1072.65170
- [15] A. Nieslony and G. Steidl, *Approximate factorizations of Fourier matrices with nonequispaced knots*, Linear Algebra Appl. **366** (2003), 337–351. MR 2004e:15016 Zbl 1018.65154
- [16] D. Potts, G. Steidl, and A. Nieslony, *Fast convolution with radial kernels at nonequispaced knots*, Numer. Math. **98** (2004), no. 2, 329–351. MR 2005f:65184

- [17] D. Potts, G. Steidl, and M. Tasche, *Fast Fourier transforms for nonequispaced data: a tutorial*, Modern sampling theory, Appl. Numer. Harmon. Anal., Birkhäuser Boston, Boston, MA, 2001, pp. 247–270. MR MR1865690
- [18] M. Schmitt, *On the sample complexity for neural trees*, Algorithmic learning theory (Otzenhausen, 1998), Lecture Notes in Comput. Sci., vol. 1501, Springer, Berlin, 1998, pp. 375–384. MR MR1683440
- [19] R. Van de Walle, H. H. Barrett, K. J. Meyers, M. I. Altbach, B. Desplanques, A. F. Gmitro, J. Cornelis, and I. Lemahieu, *Reconstruction of mr images from data acquired on a general nonregular grid by pseudoinverse calculation*, IEEE Trans. Med. Imaging **19** (2000), 1160–1167.
- [20] R. C. Wittmann, B. K. Alpert, and M. H. Francis, *Near-field antenna measurements using nonideal measurement locations*, IEEE Trans. Antennas Propagat. **46** (1998), 716–722.

Received November 30, 2005.

LESLIE GREENGARD: greengard@cims.nyu.edu
Courant Institute, New York University, New York, NY 10012, United States

JUNE-YUB LEE: jy1lee@ewha.ac.kr
Department of Mathematics, Ewha Women's University, Seoul 120-750, Korea

SOUHEIL INATI: souheil.inati@nyu.edu
Center for Neural Science and Department of Psychology, New York University,
New York, NY 10003, United States

